# Solution Self-Assembly of ABC Triblock Terpolymers with a Central Crystallizable Poly(ferrocenyldimethylsilane) Core-Forming Segment

Alex M. Oliver,[‡†] Richard J. Spontak,[§] and Ian Manners[†‡*]

[†] School of Chemistry, University of Bristol, Bristol, BS8 1TS, UK

[‡] Department of Chemistry, University of Victoria, Victoria, British Columbia V8W 3V6, Canada

[§] Departments of Chemical and Biomolecular Engineering and Materials Science and Engineering, North Carolina State University, Raleigh NC 27695, USA

[*] To whom correspondence should be addressed, e-mail: ian.manners@bristol.ac.uk or imanners@uvic.ca

**Abstract**

The synthesis and solution self-assembly behavior of a range of linear ABC triblock terpolymers (triBCPs) with a central crystallizable poly(ferrocenyldimethylsilane) (PFDMS) core-forming segment have been explored. Two different PIP-*b*-PFDMS-*b*-PMMA triBCPs (**1** and **2**) (PIP = polyisoprene, PMMA = poly(methyl methacrylate) with different block ratios (**1**: 6.2 : 1.0 : 7.6; **2**: 1.2 : 1.0 : 1.9) were investigated. TriBCP **1** was shown to form either cylinders or a mixed morphology of spheres and cylinders in various selective solvents whereas triBCP **2** yielded either network structures or platelets. The PFDMS core-forming block of the spheres of **1** and network micelles of **2** formed in hexanes appeared to undergo slow crystallization, leading to the slow transformation to form cylinders and platelets, respectively. The self-assembly behaviour of a PS-*b*-PFDMS-*b*-PMVS triBCP (**3**, block ratio: 7.9 : 1.0 : 5.7; PS = polystyrene, PMVS = poly(methylvinylsiloxane) was also examined in various solvents and yielded spheres and/or cylindrical micelles showing behavior reminiscent of **1**. Despite their disparate self-assembly behavior, seeded growth "living crystallization-driven self-assembly" methods were successfully developed for **1** – **3** using short fibers of PFDMS diBCPs as initiators to generate cylindrical B-A-B

block co-micelles with controlled lengths. Moreover, a "patchy" coronal structure for the B segments was revealed by TEM and AFM analysis of dried samples.

## Introduction

Solution-phase self-assembly of block copolymers (BCPs) is a powerful and well-established method for the preparation of a wide variety of micellar nanostructures with potential for a diverse range of applications.[1-5] Recent advances in polymer synthesis have allowed access to complex BCP materials with tailored block chemistries, such as triblock terpolymers (triBCPs), multiarm star polymers, dendritic polymers, and brush BCPs.[1-7] In turn, these advances have enabled the formation of various micelle architectures, ranging from simple core-shell systems to more complex structures, including multicompartment nanostructures with a phase-separated core or corona.[8-14] These phase-separated structures are especially desirable due to their precise, spatially-distinct functionality contained within well-defined micelle segments. Such control could allow specific post-self-assembly processes or chemistries to take place with spatial control. As a result, such architectures are of particular interest due to their ability to undergo hierarchical self-assembly,[15-17] and have a number of potential applications, including in drug delivery,[18-20] as stabilisers[21, 22], hybrid materials,[23, 24] and in catalysis[25] and optoelectronics.[3, 26]

Recent developments in BCP solution self-assembly have established that the integration of a crystallizable block affords an attractive strategy by which to prepare non-spherical nanoparticles. This process is known as "crystallization-driven self-assembly" (CDSA).[27-30] Generally, when the core-to-corona block ratio is ca. 1 : 5 – 1 : 20, cylindrical micelles are formed, whilst platelets form at block ratios closer to 1 : 1.[28] CDSA been reported for a variety of crystallizable polymers,[29, 31-35] including conjugated materials,[36-38] and molecular species that self-assemble by non-covalent π-stacking interactions.[39, 40] In collaboration with Winnik and coworkers we have shown that a key advantage of CDSA over the self-assembly of BCPs with an amorphous core-forming block is that the termini of many micelles with crystalline cores remain active towards the addition of further incoming BCP unimer via an epitaxial growth mechanism. This process, termed "living CDSA", is analogous to

living covalent polymerization of molecular monomers.[41, 42] This enables the formation of micelles in both 1D and 2D with precise control over the micelle dimensions and results in samples with low length and area dispersities.[42, 43] Furthermore, this methodology has opened convenient routes towards the formation of more complex architectures such as block co-micelles,[42] block co-platelets,[43] "patchy" micelles,[44-46] and hierarchical structures.[47-49] Living CDSA has been reported for a range of crystallizable core-forming blocks, including PFDMS,[50] polyethylene,[51] polylactide,[52] poly(ε-caprolactone),[53] conjugated polymers such as poly(3-hexylthiophene),[54] poly(3-decylselenophene),[55] and oligo(*p*-phenylenevinylene),[56-58] poly(dialkylfluorene)[59] as well as molecular species that self-assemble via non-covalent interactions.[39, 60-62]

Several recent studies describe the formation of triBCP micelles with a crystallizable core and controlled lengths that also exhibit phase-separated, or "patchy", coronal structures. Schmalz and co-workers have reported the preparation of micelles with a crystallizable polyethylene (PE: polyethylene) core and a phase-segregated corona produced by the CDSA of a polystyrene-*b*-PE-*b*-poly(methylmethacrylate) (PS-*b*-PE-*b*-PMMA) triBCP.[29, 63] Both cylindrical and spherical micelles with a phase-separated PS/PMMA corona could be obtained depending on the quality of the solvent for the core-forming PE block. Living CDSA of the triBCP in the presence of seeds was shown to afford cylindrical micelles with controlled lengths and coronal microphase separation.[51] Moreover, it has been reported that an analogous system with a PFDMS core-forming block, PS-*b*-PFDMS-*b*-PMMA, afforded cylindrical micelles that also exhibit a patchy coronal microstructure.[44] In both these cases, the coronal patchiness was attributed to immiscibility between the PS and PMMA corona-forming blocks. However, neither PS nor PMMA contain any functional groups that allow further chemical modification, such as complexation of specific patches with nanoparticles, which could lead new avenues for applications.

With this in mind, recent work from Schmalz, Greiner and co-workers has focused on the preparation of patchy micelles with functional PMMA coronal domains that could be easily tailored using tertiary amino groups as a versatile route to mesostructured hybrid materials.[64] The CDSA of a functionalized PS-*b*-PE-*b*-PMMA triBCP and consequent definition of the patchiness of the self-

assembled micelles was found to strongly depend on the polarity and solubility of the amidated PMMA block. Furthermore, the micelles were used as templates for the selective incorporation of Au nanoparticles within the amidated PMMA coronal patches. These hybrid materials have been used in the preparation of patchy non-woven fibre mats by coaxial electrospinning with PS, and have been shown to be effective as heterogeneous catalytic supports.[25]

Additional examples of PFDMS-based materials that exhibit phase-segregated coronal structures have also been reported. Seeded co-assembly of linear and functionalized-brush PFDMS-*b*-poly(methylvinylsiloxane) (PFDMS-*b*-PMVS) BCPs yields the formation of gradient-type cylindrical micelles with a phase-separated corona.[45] Recent work has also demonstrated the formation of "patchy" structures through the co-assembly of PFDMS-*b*-poly(2-vinylpyridine) (PFDMS-*b*-P2VP) and PFDMS-*b*-poly(N-isopropylacrylamide) (PFDMS-*b*-PNIPAM) BCPs using living CDSA.[30] Furthermore, a PFDMS-containing miktoarm star polymer, PS-*arm*-polyisoprene-*arm*-PFDMS (PS-*arm*-PIP-*arm*-PFDMS), also formed cylinders with phase-separated PS and PIP corona-forming blocks.[46] However, the ability to prepare patchy micellar materials via living CDSA and subsequent functionalization with nanoparticles, and their ensuing use for applications such as catalysis, has not been explored in detail.[65, 66] As a follow up to our recent investigation of the self-assembly of PS-*b*-PFDMS-*b*-PMMA triBCPs that self-assemble into "patchy" cylindrical micelles,[44] in the present work, we report the synthesis and self-assembly of several new PFDMS-containing triBCPs with various other corona-forming blocks. This work aims to expand the library of "patchy" PFDMS micellar materials. Furthermore, our attempts to control the micelle dimensions through seeded growth is also discussed.

## Results and Discussion

### *Synthesis of ABC Triblock Terpolymers with a PFDMS Core-Forming "B" Block*

A series of ABC triBCPs with a central PFDMS core-forming (B) block and two chemically distinct corona-forming (A and C) blocks was prepared through various different methods, including living anionic polymerization, living radical polymerization and copper azide/alkyne cycloaddition

(CuAAC) click chemistry. Different corona-forming blocks were selected to induce the formation of phase-separated microstructures during self-assembly. The characterization data of all triBCPs studied, and their relative homopolymer/BCP constituents, are summarised in Table 1 and Table S1, respectively.

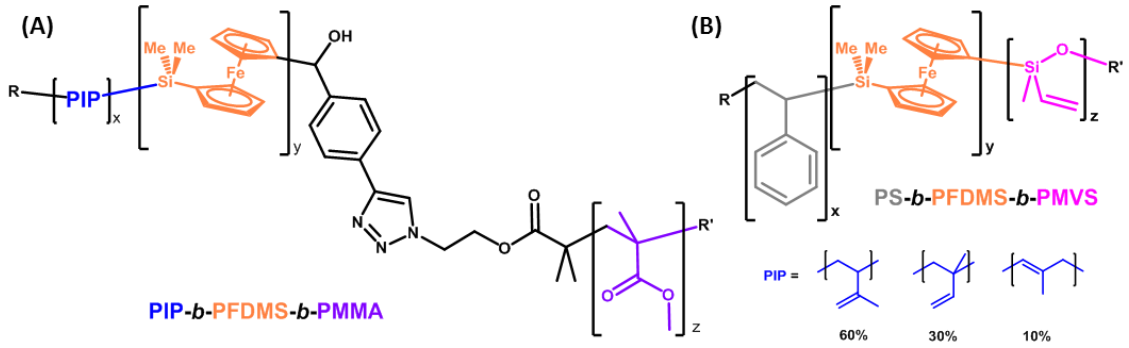


**Scheme 1**: Chemical structures of (A) – PIP-*b*-PFDMS-*b*-PMMA and (B) PS-*b*-PFDMS-*b*-PMVS triBCPs.

Two PIP-*b*-PFDMS-*b*-PMMA triBCPs (**1**, **2**), as depicted in Scheme 1A, with different block lengths, were prepared by a combination of living anionic polymerization, atom-transfer radical polymerization (ATRP), and CuAAC click chemistry (Scheme S1). A PS-*b*-PFDMS-*b*-PMVS triBCP (**3**), as shown in Scheme 1B, was prepared using solely sequential living anionic polymerization (Scheme S2). The crude materials were purified by precipitation and preparative size-exclusion chromatography, affording the final triBCPs as orange solids in moderate-to-good yields (**1**: 32%, **2**: 44%, **3**: 82%). Characterization of triBCPs was achieved through a combination of gel permeation chromatography (GPC), $^{1}$H NMR spectroscopy, and matrix-assisted laser desorption/ionization time-of-flight (MALDI-TOF) mass spectrometry. GPC analysis confirmed that all the triBCPs and their constituent homopolymers and BCPs possessed narrow molecular weight distributions (PDI < 1.12) (Figure S1 – Figure S3). The block ratios of the synthesised triBCPs were determined by $^{1}$H NMR through comparative integration of specific peaks distinctive to each block (the aryl peaks on PS (δ =

6.41-7.21), the cyclopentadienyl protons of PFDMS (δ = 4.12, 4.28), the methoxy peaks on PMMA (δ = 3.59), the vinylic peaks of PIP (δ = 4.70-6.16) and the methyl peaks of PMVS (δ = 0.16)). This data was used in conjunction with the absolute molecular weights of the PS block as determined by GPC using a triple detector array, and corroborated with MALDI-TOF mass spectroscopy, to give the composition of the final materials.

**Table 1**: Characterization data of ABC triBCPs prepared, including number-average molecular weight ($M_n$), degree of polymerization ($DP_n$), block ratio and polydispersities (PDI).

| Composition [a,b] | triBCP | Block Ratio A : B : C [a] | Total Core : Corona Ratio [a, c] | $M_n$ / kg•mol$^{-1}$ [b] | PDI [b] |
|---|---|---|---|---|---|
| $PIP_{313}$-*b*-$PFDMS_{50}$-*b*-$PMMA_{381}$ | **1** | 6.2 : 1.0 : 7.6 | 1.0 : 13.8 | 60.0 | 1.12 |
| $PIP_{46}$-*b*-$PFDMS_{39}$-*b*-$PMMA_{75}$ | **2** | 1.2 : 1.0 : 1.9 | 1.0 : 3.1 | 22.2 | 1.05 |
| $PS_{340}$-*b*-$PFDMS_{43}$-*b*-$PMVS_{247}$ | **3** | 7.9 : 1.0 : 5.7 | 1.0 : 13.6 | 82.6 | 1.08 |

[a] Determined by $^1$H NMR through comparative integration of vinylic protons (2.2H) of PIP, cyclopentadienyl protons (2 x 4H) of PFDMS, methoxy protons (3H) of PMMA, aromatic protons (5H) of PS and methyl peaks (3H) of PMVS (depending on the triBCP composition), [b] Determined by GPC with a triple-detector array, [c] Molar ratio.

*Self-Assembly of PIP-b-PFDMS-b-PMMA Triblock Terpolymers*

*(a) Self-Assembly of $PIP_{313}$-b-$PFDMS_{50}$-b-$PMMA_{381}$ (**1**)*

The first material studied was $PIP_{313}$-*b*-$PFDMS_{50}$-*b*-$PMMA_{381}$, **1**, (subscripts denote $DP_n$ for each block) with a core (B) to total coronal (A and C) block ratio of 1.0 : 13.8. THF was used as a common solvent for all 3 blocks, and several selective solvents in which PFDMS is insoluble were studied. Both non-polar solvents (such as hexanes and decane) which are better solvents for the PIP block, as well as more polar solvents (such as acetone) which are more selective for the PMMA block were systematically explored. In addition, ethyl acetate (EtOAc, which should be a good solvent for both corona-forming blocks was investigated (for reference, see Table S2 for relative solvent solubility parameters). In typical self-assembly experiments, samples were prepared by addition of a triBCP unimer solution (10 mg/mL in THF) at ambient temperature to the desired selective solvent, resulting in a final solution concentration of 0.1 mg/mL. Each solution was heated to ca. 1 °C below the boiling point of the solvent (Table S3) for 1 h, and then left to slowly cool (rate ≈ 1 °C/min) to room

temperature, after which the solutions were matured for a minimum of 24 h. The resulting micellar solutions were analyzed using transmission electron microscopy (TEM) by drop-casting ca. 10 μL of the colloidal suspension onto carbon-coated copper grids, followed by subsequent solvent evaporation.

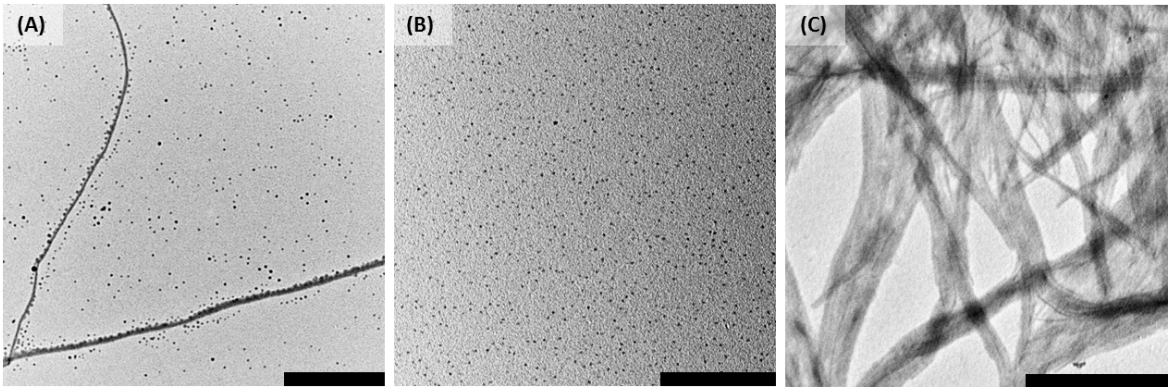


**Figure 1**: TEM micrographs of triBCP micelles of **1** prepared in, and drop-cast from, (A) hexanes, (B) decane and (C) acetone. TEM images taken after drying from solution at 0.1 mg/mL. Scale bars correspond to 1000 nm.

Using this protocol, a mixture of spheres and very long cylinders was observed when hexanes was used as a solvent (Figure 1A), whilst in decane only spherical micelles were detected (Figure 1B). Ageing of the samples in hexanes and decane for longer periods of time (> 3 months) showed partial evolution of the micellar morphologies from spheres to cylinders (Figure S5). This morphological transformation could be attributed to the solvent present allowing the slow crystallization of the PFDMS, resulting in a gradual transition from spheres to cylinders. It is plausible that a mixed amorphous core composed of PFDMS and PMMA is obtained initially for the spherical micelles formed in both cases, together with a solubilising corona of PIP. The presence of PMMA in the core would be expected to hinder the ability of the PFDMS block to crystallize. As hexane is a better solvent for PFDMS than decane (as predicted by their respectively solubility parameters, see: Table S2, S3), plasticization, which would be expected to facilitate PFDMS crystallization, should be more favoured in the former solvent. The difference in self-assembly behavior may also be partly attributed to the increased coronal volume of the PIP block when self-assembled in decane compared to hexane which would favour sphere formation. In contrast to the behavior in n-alkanes, in acetone, only

highly aggregated cylindrical micelles were afforded after drying (Figure 1C). As acetone is a better solvent for PFDMS than n-alkanes (see Table S2, S3) the formation of cylinders with a crystalline core is expected. Aggregation may be the result of a drying effect promoted by intermicellear interactions between the PIP chains which are poorly solvated in acetone. When **1** was dissolved in EtOAc, no micelles were obtained and only polymer film, presumably derived from unimer, was detected even on aging (Figure S4, S6 and S7). This is likely due to the solvent being good for both PIP and PMMA, and only a moderately poor solvent for the PFDMS core-forming block.

*(b) Seeded Growth of $PIP_{313}$-b-$PFDMS_{50}$-b-$PMMA_{381}$ (**1**)*

Seeded growth studies with **1** were conducted with the objective of accessing 1D assemblies with control over the micelle dimensions. The initial experiments used seed micelles prepared from polydisperse cylindrical micelles of **1** in acetone after sonication in order to fragment nanostructures into seeds. Seeded growth experiments were conducted in various solvent systems comprised of mixtures of acetone/decane at room temperature. However, the use of this mixture proved problematic due to incomplete unimer consumption and significant micelle aggregation. (Figure S8 – Figure S10). Thus, further investigations explored different seed/solvent combinations.

Seeded growth experiments were conducted by the addition of **1** to $PIP_{404}$-*b*-$PFDMS_{49}$ BCP seed micelles (block ratio 8.2 : 1.0, $L_n$ = 493 nm, $L_w/L_n$ = 1.03, where $L_n$ and $L_w$ denote the number- and weight-average micelle length, respectively) that were prepared in decane by sonication of a dispersion of polydisperse micelles for 2 h at 0 °C. Self-assembly solvent systems of pure decane, decane/acetone (3 : 1 (v/v)) and decane/acetone (1 : 1 (v/v)) were investigated, at a consistent unimer-to-seed ratio of 8 : 1. When pure decane was used as the selective solvent, the seed micelle length did not increase substantially ($L_n$ = 594 nm), whilst a significant amount of spheres were also formed (Figure 2A). When decane/acetone (3 : 1 (v/v)) was used, the length of the resulting cylindrical block co-micelles increased ($L_n$ = 1431 nm). However, this was much shorter than the predicted length (ca. 4400 nm), and spherical micelles were also observed by TEM (albeit in reduced amounts compared to in neat decane) (Figure 2B). In decane/acetone (1 : 1 (v/v)) the length of the micelles increased

dramatically ($L_n$ = 3868 nm) to give a value closer to the predicted length at a unimer-to-seed ratio of 8 : 1 (Figure 2C). In addition, the number of spherical micelles that could be detected was noticeably reduced. However, the length dispersity of the block co-micelles was uncharacteristically large ($L_w/L_n$ = 1.24) for micelles prepared by living CDSA. Moreover, the cylindrical block co-micelles possessed a variety of unusual shapes in the dry state as detected by TEM (Figure 2C and S14). A substantial population of the micelles appeared to possess coiled outer blocks of the block co-micelles, with a thicker dark region detected on the inside of these coils (Figure 2D). In addition, some micelles possessed straight regions with coiled ends (Figure 2C).

The interesting micelle coiling detected in decane/acetone is most likely explained as a drying effect. Acetone, a selective solvent for the PMMA block, has a significantly lower boiling point than decane (56 °C compared 174 °C). Therefore, acetone will evaporate more rapidly than decane after drop-casting. During the final stages of drying, the block co-micelles would be exposed to almost pure decane, which is a strongly selective solvent for the PIP block. In order to minimise unfavourable interactions between PMMA and decane, the block co-micelles may consequently bend as the solvent evaporates as the PMMA coronal chains collapse. Such coiling is, however, impeded by the relatively rigid crystalline PFDMS micelle core, thereby accounting for the large circumscribed radii of the coils in which the more electron dense metalloblock is located on the core periphery, as shown by TEM (Figure 2D and 3A and 3B, see green arrows). One might expect that if coiling places sufficient stress on the block co-micelles the cylinders could ultimately undergo cleavage and there is evidence for this at the co-micelle junctions (Figure S11). Consistent with this explanation, the coiling is almost entirely eliminated by the addition of a high boiling point polar selective co-solvent such as DMSO or DMF (Figure S12). Analogous self-assembly experiments were also conducted where hexanes (boiling point 70°C) was used instead of relatively involatile decane in the selective solvent mixtures and coiling was also eliminated but otherwise, similar results were observed (Figure S13 - S15).

Observation of the long straight cylindrical assemblies formed in decane/acetone mixtures under high magnification (Figure 3, red arrows) showed that these consist of two micelles that have apparently packed together upon drying. Two micelle cores with a lighter region in-between cane be

detected (Figure 3). It is likely that the aggregation is also the result of a drying effect where the PMMA coronal chains on adjacent micelles interact to minimise unfavourable interactions with the solvent.

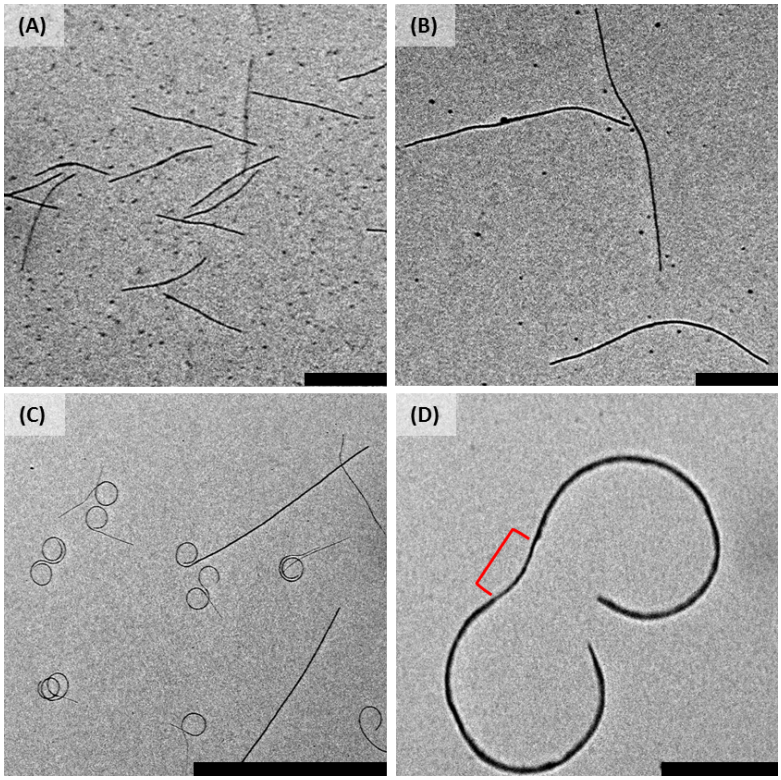


**Figure 2**: TEM micrographs of block co-micelles prepared by seeded growth of **1** from $PIP_{404}$-*b*-$PFDMS_{49}$ seed micelles in decane ($L_n$ = 493 nm, $L_w/L_n$ = 1.03) and drop-cast from various solvent systems; (A) a mixture of spherical and cylindrical micelles in decane; (B) a mixture of spherical and slightly longer cylindrical micelles in decane/acetone (3 : 1 (v/v)); (C) cylinders in decane/acetone (1 : 1 (v/v)) showing a variety of coiled and straight dried structures; (D) a higher magnification micrograph of one of the coiled block co-micelles TEM images taken after drying from solution at 0.1 mg/mL (red bracket denotes the seed micelle). Scale bars correspond to (A)-(B), (D) 500 nm, (C) 5000 nm.

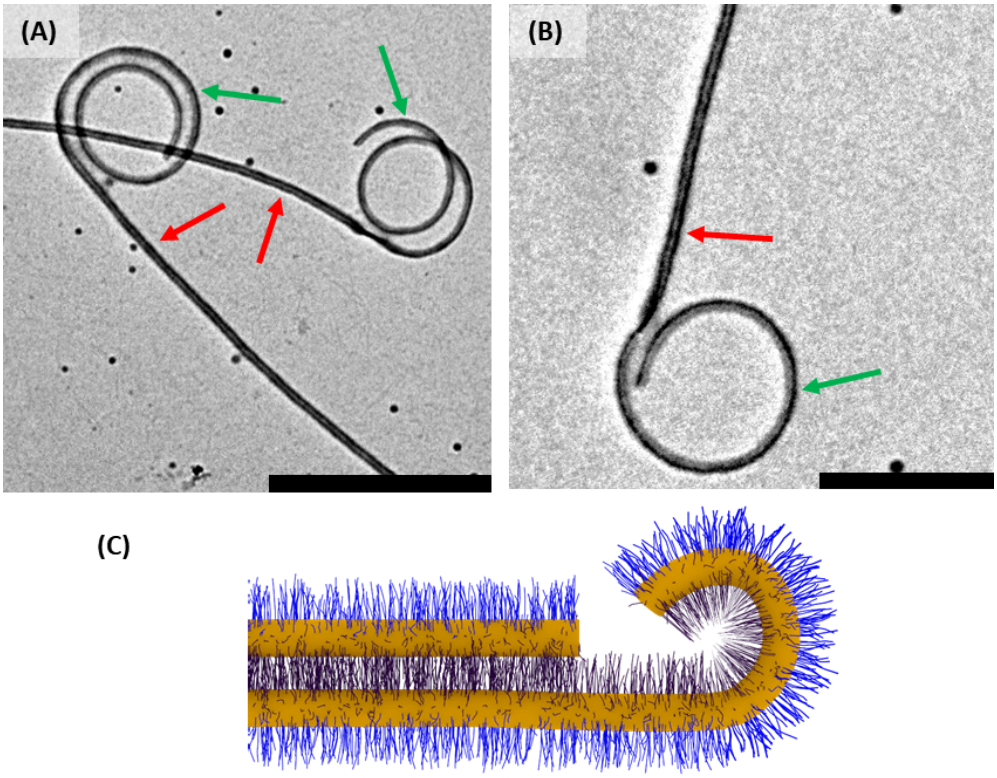


**Figure 3**: (A), (B) TEM micrographs of the ends of two block co-micelles prepared by seeded growth of **1** from $PIP_{404}$-*b*-$PFDMS_{49}$ seed micelles in decane ($L_n$ = 493 nm, $L_w/L_n$ = 1.03) and drop-cast from decane/acetone (1 : 1 (v/v)) showing the packing of two block co-micelles together to minimise unfavourable interactions between decane and the PMMA corona-forming blocks. When only one block co-micelle is present, the micelle coils upon itself to minimise the unfavourable solvent interactions upon solvent evaporation (red arrows denote packing of two micelles, green arrows denote micelle coiling); (C) is a simplified schematic representation of this structure, whereby block co-micelle outer blocks either pack together, or bend to minimise unfavourable interactions of the PMMA corona chains with decane (PMMA = purple corona, PIP = blue corona). TEM images taken after drying from solution at 0.1 mg/mL. Scale bars correspond to 500 nm.

Finally, the use of PFDMS-*b*-PDMS seed micelles in EtOAc was investigated for the seeded growth of triBCP **1** (Figure 4). In this case, EtOAc was used as a selective solvent over a less polar solvent such as hexanes (which is typically used for PFDMS-*b*-PDMS self-assembly) as it is a good solvent for both the PMMA and PIP blocks. Self-assembly in EtOAc is typically slower than in less polar solvents such as hexanes as EtOAc is only moderately poor for the PFDMS core-forming block.[67, 68] $PFDMS_{52}$-*b*-$PDMS_{414}$ seed micelles (block ratio 8.0 : 1.0, $L_n$ = 49 nm, $L_w/L_n$ = 1.10) were prepared by sonication of a solution of long polydisperse micelles formed by self-nucleation in EtOAc for 2 h at 0 °C. The micelle solutions prepared by the addition of known amounts of unimer to the

seed micelles in EtOAc, and the samples were allowed to age for 72 h to ensure that the living growth process could proceed to completion.

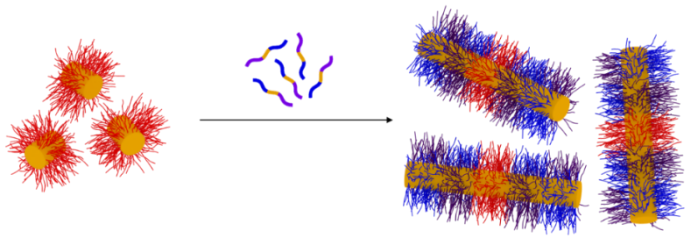

**Figure 4**: Schematic representation of the formation of block co-micelles of **1** grown off PFDMS-*b*-PDMS seed micelles.

The length of the micelles was shown to increase linearly as the amount of unimer of **1** increased, and micelles up to ca. 1000 nm with low length dispersities ($L_w/L_n$ < 1.1) were afforded (Figure 5A, 5B, Figure S16). Micelle lengths correlated favourably with the predicted micelle lengths depending on the unimer-to-seed ratio, inferring that living CDSA was taking place (Figure 5D, Figure S17). In addition, no spherical micelles were detected, as was observed in the presence of *n*-alkane solvents (Figure 2). This is indicative that using a solvent that is good for both corona forming blocks is preferred for the formation of monodisperse nanostructures via living CDSA of **1**. In the case of EtOAc this is quite remarkable as attempted self-assembly of **1** in EtOAc in the absence of seed micelles resulted in only a film derived from unassembled unimer being observed. The presence of a preformed crystal nucleus for the growth of **1** is extremely important for this triBCP to self-assemble effectively. Furthermore, no coiling of the micelles was observed upon drying, which was in stark contrast to the block co-micelles prepared in decane/acetone mixtures (Figure 2). This is presumably due to the use of a selective solvent (EtOAc) that is good for both PIP and PMMA. The micelles were also characterized by AFM which also revealed cylindrical micelles with low length dispersities (Figure 5C).

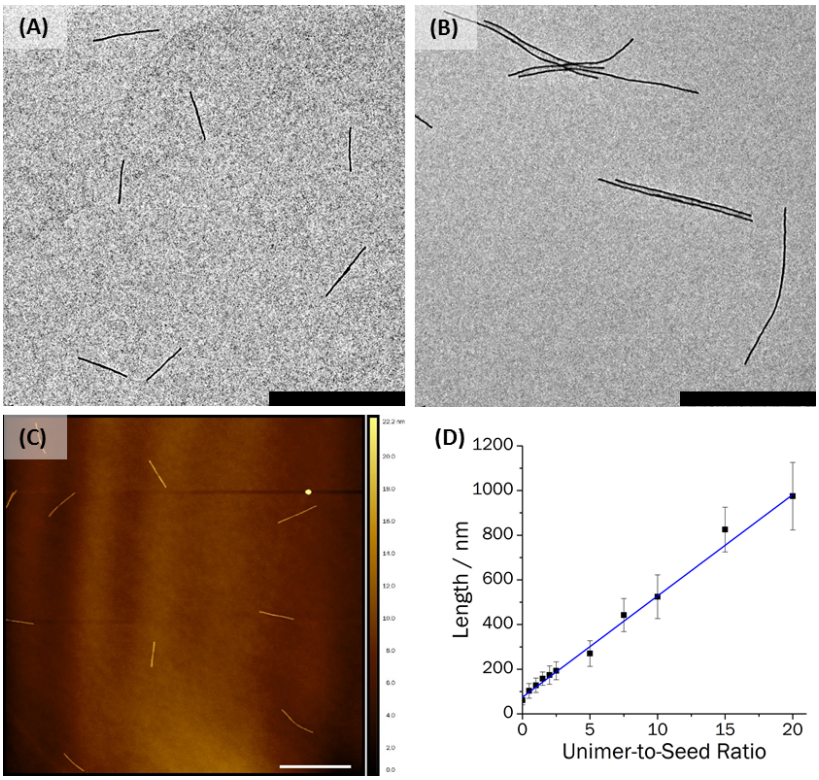


**Figure 5**: TEM micrographs of cylindrical block co-micelles prepared by seeded growth of **1** from $PFDMS_{52}$-*b*-$PDMS_{414}$ seed micelles ($L_n$ = 49 nm, $L_w/L_n$ = 1.10) in EtOAc after the addition of (A) 7.5 and (B) 20 equivalents of unimer; (C) AFM height micrograph of the same cylindrical block co-micelles as in (B) after the addition of 20 equivalents of unimer; (D) Graph showing the linear dependence of micelle length upon the unimer-to-seed ratio. TEM and AFM images taken after drying from solution at 0.1 mg/mL. Scale bars correspond to (A), (B) 1000 nm, (C) 2000 nm.

After preparing well-defined 1D assemblies using **1**, the presence of microphase separation between the corona-forming blocks of the micelles was interrogated by TEM and AFM. For TEM, freshly drop-cast samples of block co-micelles were exposed to $OsO_4$ vapour for ca. 16 h prior to imaging to selectively stain the PIP coronal chains. An irregular phase-separated coronal structure was detected in the dry state, consisting of PIP (dark due to staining with Os) and PMMA (light) traversing the length of the block co-micelle outer blocks (Figure 6A). Moreover, the staining process aided in showing the clear formation of block co-micelle structures, as $OsO_4$ does not stain the PDMS corona of the seed micelle. Furthermore, imaging by AFM confirmed the formation of an irregular patchy structure (Figure 6B). Patchy coronal protrusions were observed along the length of the outer blocks of the block co-micelles by AFM. Likewise, height profiles along the length of the outer

blocks show irregular heights profiles when measuring along the micelle corona, further substantiating the formation of a patchy corona (Figure 6C).

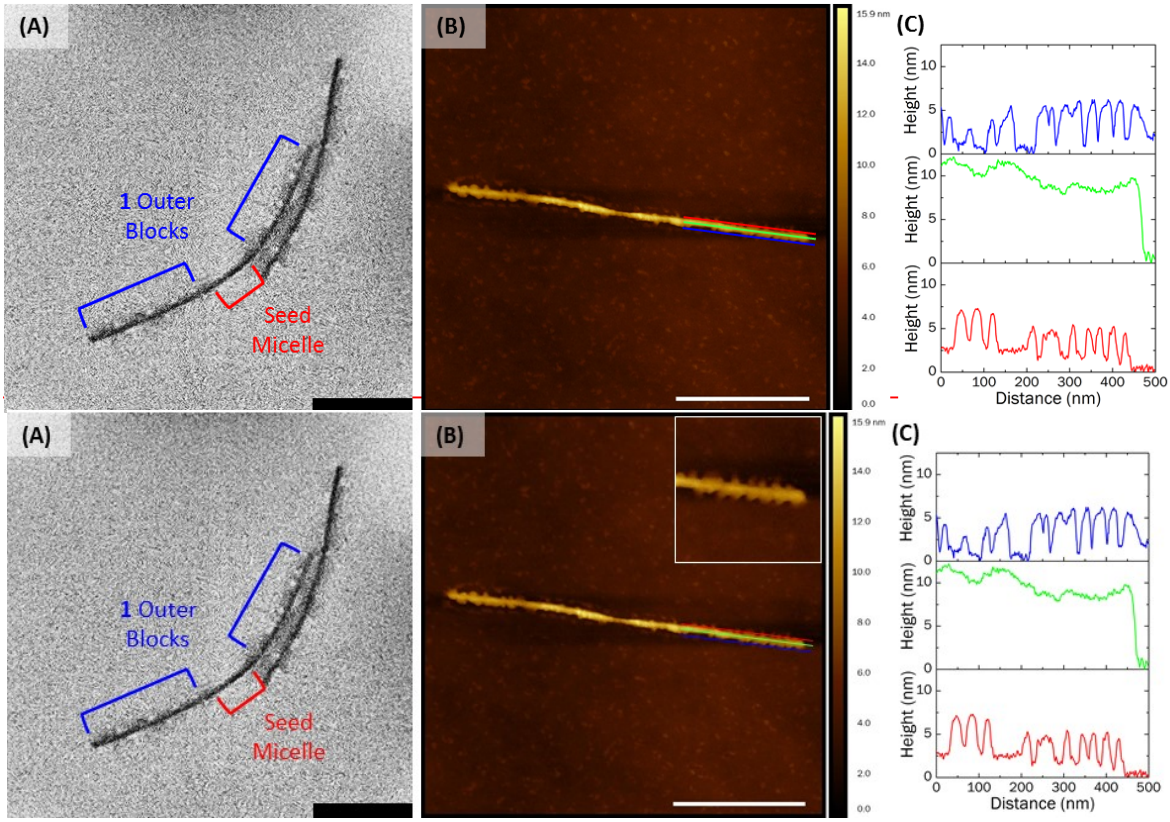


**Figure 6**: (A) TEM micrograph and (B) AFM height micrograph of cylindrical block co-micelles prepared by seeded growth of **1** from $PFDMS_{52}$-*b*-$PDMS_{414}$ seed micelles ($L_n$ = 49 nm, $L_w/L_n$ = 1.10) in EtOAc showing a "patchy" structure with phase-segregated PIP and PMMA coronal chains upon solvent evaporation in the dry state (see inset for higher magnification of the outer block of the triblock co-micelle outlining the irregular dry state coronal structure); (C) representative height profiles taken from (B) of different parts along the length of a "patchy" block co-micelle in the dry state. TEM and AFM images taken after drying from solution at 0.1 mg/mL. TEM image was taken after exposure to $OsO_4$ vapour. Scale bars correspond to (A) 200 nm, (B) 500 nm.

As noted above, coiling of these block co-micelles prepared in EtOAc (boiling point 77 °C) was not detected on solvent evaporation. We therefore explored whether this coiling effect could be induced through the addition of the high boiling point solvent decane, which is poor for PMMA. A solution of block co-micelles in EtOAc ($L_n$ = 975 nm) was diluted in decane, which is selective for both PIP and PDMS (from the seed) to give final solvent mixtures of decane/EtOAc 1 : 3 (v/v) and 1 : 1 (v/v). However, in this case on solvent evaporation, instead of micelle coiling, mainly end-to-end

micelle aggregation was detected after solvent evaporation by TEM analysis (Figure S19), with the degree of aggregation increasing with a greater decane fraction. Although further detailed studies of these phenomena are clearly needed, the difference from the previously observed micelle coiling in decane/acetone (Figure 2C, 2D, and 3) may be the result of the difference in size of the coronal patches formed in the different solvent media or the significant difference in boiling points between the two solvents present in each case which leads to different relative rates of evaporation (EtOAc has a boiling point ca. 20°C higher than acetone).

*(c) Self-Assembly of $PIP_{46}$-b-$PFDMS_{39}$-b-$PMMA_{75}$ (**2**)*

In order to determine how changing the length of the corona-forming blocks affected the solution self-assembly of PIP-*b*-PFDMS-*b*-PMMA triBCPs we also investigated the behavior of $PIP_{46}$-*b*-$PFDMS_{39}$-*b*-$PMMA_{75}$ (**2**). TriBCP **2** possesses significantly shorter corona-forming block lengths than **1**, with a core to total-corona-forming block ratio of 1.0 : 3.1 (compared to 1.0 : 13.8 in **1**). The difference in composition was expected to lead to a preference for the formation of structures with more 2D character due to the reduction in inter-coronal chain repulsion from the shorter PIP and PMMA corona-forming blocks.[28] Self-assembly studies were conducted under analogous conditions to those used for **1**.

Interestingly, when **2** was self-assembled in hexanes, ~~bi~~continuous ~~type~~ network~~s~~ of micelles were detected by TEM (Figure 7A, 7D). Similar structures were observed when decane was used as the selective solvent. (Figure 7B, 7E). Some of the observed network micelles were several microns across, whilst smaller fragments were also detected. The micelles were also imaged by AFM in the dry state, revealing the presence of intricate ~~bicontinuous~~ networks throughout (Figure 8, S21). These structures resemble those formed by BCPs with amorphous core-forming blocks and indicates that the PFDMS and presumably PMMA form a core in which the former does not crystallize.[3] In contrast, self-assembly in acetone led to the formation of highly aggregated platelet and cylindrical micelles upon drying which presumably possess crystalline PFDMS cores (Figure 7C, 7F), whilst in EtOAc, only a film, presumably derived from unimer, was detected (Figure S20A). The behavior of **2** in

acetone and EtOAc is reminiscent of that for triBCP **1** except that 2D structures are also formed in the former case.[28]

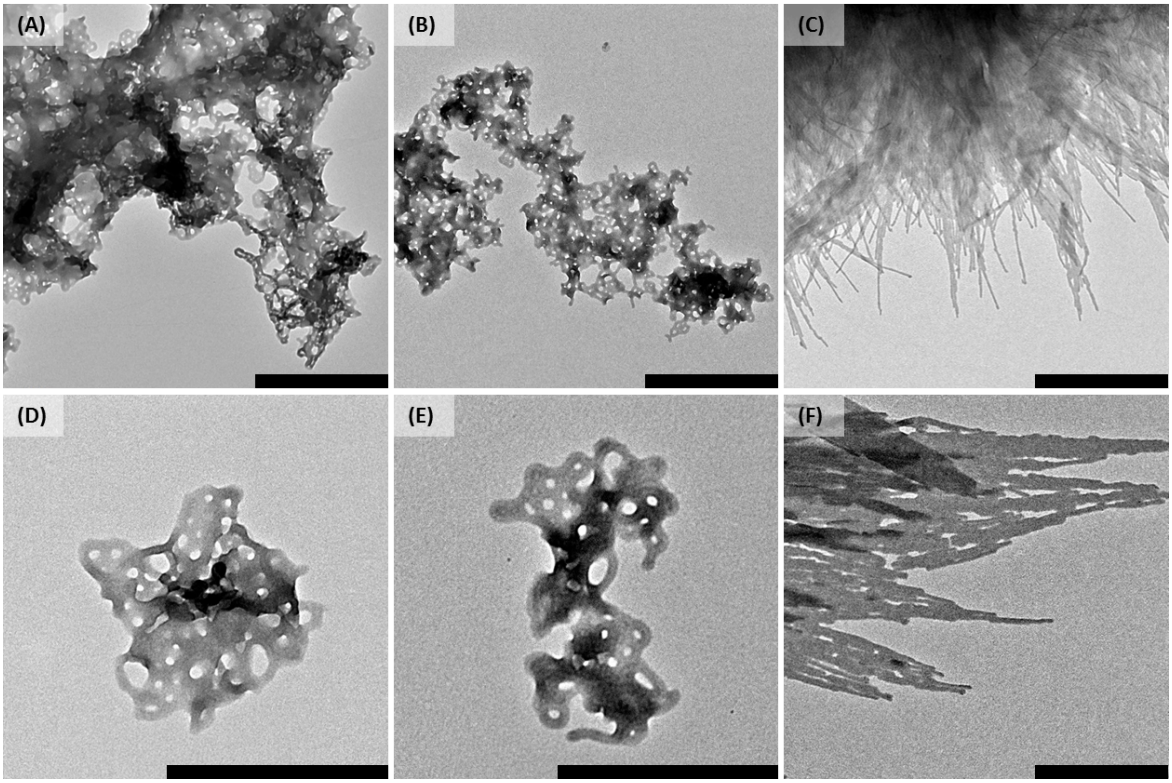


**Figure 7**: TEM micrographs ((A)-(C) low magnification and (D)-(F) high magnification) of triBCP micelles of **2** prepared in, and drop-cast from, (A), (D) – hexanes, (B), (E) – decane and (C), (F) – acetone. TEM images taken after drying from solution at 0.1 mg/mL. Scale bars correspond to (A)-(C) 1000 nm, (D)-(F) 500 nm.

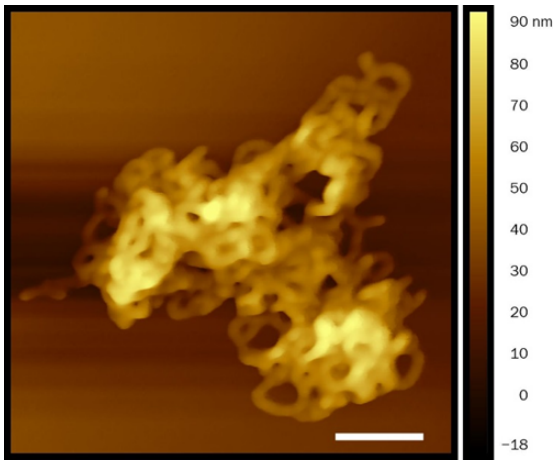

**Figure 8**: AFM micrograph of triBCP micelles of **2** prepared in, and drop-cast from, decane. AFM image taken after drying from a solution at 0.1 mg/mL. Scale bar corresponds to 500 nm.

The network-type structures are of particular interest as they are a morphology for self-assembled PFDMS BCPs that has not been prepared previously. These large structures were shown by DLS to be present in solution and their formation therefore is not merely a drying effect. Thus, assemblies with a apparent hydrodynamic radius, $R_{h,app}$, of ca. 1600 nm were detected after brief sonication (Figure S22), which was necessary as the original assemblies with $R_{h,app} > 10$ μm could not be accurately analyzed by DLS.

A more detailed 3D analysis of dried network nanostructures formed by triBCP **2** in the presence of decane were performed by transmission electron microtomography (TEMT).[69-71] Aligned TEM images were collected at tilt angles ranging from 0° to 40° in 10° intervals (Figure S23A), which confirmed that these micellar networks possess a highly irregular topology, as well as flexible cylindrical micelles along the thinner periphery, in agreement with AFM height images (Figure 8). Reconstruction of images acquired at tilt angles from –64.5° to +64.5° in 1.5° intervals by the *r*-weighted (or filtered) back-projection method[72] yielded a 3D volume element in which the *x*-*y* plane is perpendicular to the electron beam along the *z*-axis. Sequential *x*-*y* slices provided a walk-through of the solid (Figure S23B), decreasing from the top of the specimen in 10 nm increments. Careful comparison of the TEM image at 0°, an *x*-*y* slice of the reconstruction at the carbon surface and two enlargements of the identified region at different *z* heights corroborated the presence of internal structure within the network specimen (Figures 9). A 3D representation of the reconstructed volume element displayed at discrete tilt angles of –30°, 0° and 30° (Figure 10) and continuously from 0° to 360° (Movie S1) revealed the existence of highly curved cylindrical and spherical micelles within the network, suggesting that, whilst these micellar networks form in solution, they are not at thermodynamic equilibrium.

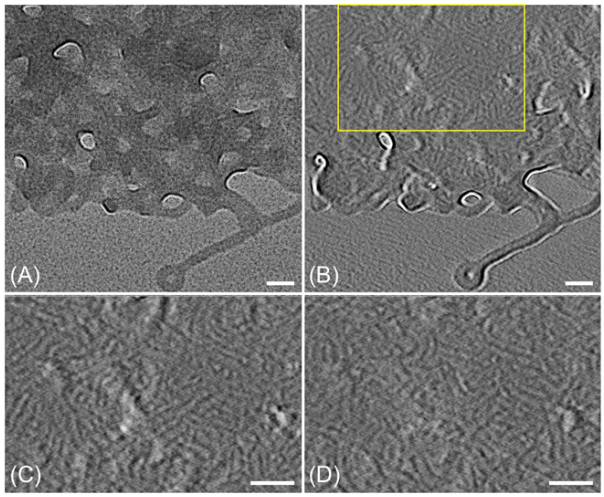


**Figure 9**: (A) TEM and (B-D) TEMT images of a cylindrical triBCP micelle network of 2 prepared in, and drop-cast from, decane after drying from solution at 0.1 mg/mL. The TEM image in (A) has been acquired at 0° tilt. The TEMT image in (B), as well as the enlargement of the framed region in (C), represents an x-y slice of the 3D volume reconstruction near the plane of the substrate. The TEMT image in (D) is an x-y slice of the same region at 10 nm below the one in (C). Scale bars correspond to 100 nm.

The samples in hexanes and decane were matured for 3 weeks and were subsequently reimaged. A mixed morphology was observed in hexanes, with both network and platelet structures being detected (Figure S24B). The formation of these platelet micelles is presumably a direct result of crystallization of the PFDMS core-forming block. This process is analogous to previous work that was reported with PFDMS-*b*-poly(2-vinylpyridine) (PFDMS-*b*-P2VP) BCPs, where a slow transition from spheres to cylinders was observed over time in a poor solvent for the core-forming block.[73] However, for samples prepared in decane, the ~~bicontinuous~~network structures were kinetically trapped with no discernible morphological evolution perceived over the course of 3 weeks (Figure S24E). To this end, the micelle solutions were reimaged after ageing for 9 months, after which only platelet micelles were detected in hexanes (Figure S24C), and unchanged network structures were observed in decane (Figure S24F). Moreover, samples in EtOAc had not altered either, with only film presumably derived from unimer being detected (Figure S20B).

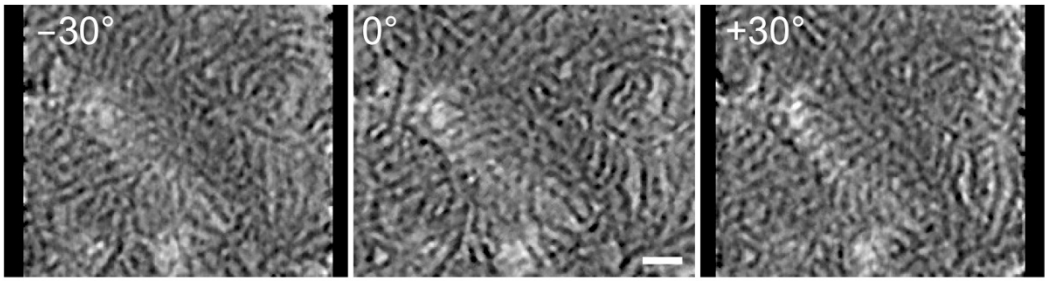


**Figure 10**: Three views at different projection angles (labelled) of a 3D tomographic reconstruction of a cylindrical triBCP micelle network of 2 prepared in, and drop-cast from, decane after drying from solution at 0.1 mg/mL. A 360° movie clip of this reconstruction is available in the Supporting Information (Movie S1). Scale bar corresponds to 50 nm.

*(d) Seeded Growth of $PIP_{46}$-b-$PFDMS_{39}$-b-$PMMA_{75}$ (**2**)*

Seeded growth experiments with triBCP **2** were likewise conducted in order to control the dimensions of the resulting micelles. $PFDMS_{52}$-*b*-$PDMS_{414}$ seed micelles in EtOAc were used and the experimental conditions were the same as outlined previously for **1**. The micelles increased in length as the unimer-to-seed ratio increased (Figure S25A-E), and micelles up to ca. 1100 nm were accessible. Furthermore, this length increase was linearly related amount of **2** unimer that was added (Figure S25F, Figure S26). The prominent morphology for the afforded micelles was cylindrical, however some core thickening and branching were also detected by TEM at higher unimer-to-seed ratios (Figure S27). This is presumably due to the low core to corona block ratio (1.0 : 3.1) for **2**, which may be at the threshold block ratio between the formation of 1D cylinders and 2D platelets.[28] This observation is also similar to that observed for the seeded growth PS-*b*-PFDMS-*b*-PMMA triBCPs that have a comparable core to corona block ratio.[44] These near monodisperse block co-micelles and some branched micelles were also imaged by AFM in the dry state (Figure S28). As a comparison, seeded growth experiments were also conducted using seed micelles prepared from polydisperse cylinders of **2** in acetone. In marked contrast to the cylindrical micelles that developed from $PFDMS_{52}$-*b*-$PDMS_{414}$ seed micelles in EtOAc, poorly defined lenticular platelet micelles form in this case and these increased in area as the unimer-to-seed ratio increased (Figure S29). However, the

platelets extensively aggregated upon drying which made a quantitative analysis of the micelle areas impossible.

*(e) Self-Assembly of $PS_{340}$-b-$PFDMS_{43}$-b-$PMVS_{247}$ (3)*

In a final set of experiments, the self-assembly behaviour of $PS_{340}$-*b*-$PFDMS_{43}$-*b*-$PMVS_{247}$, triBCP **3**, was studied. This material had a core to total-corona-forming block ratio of 1.0 : 13.6, similar to that of **1**, but with two different corona-forming blocks (PS and PMVS). As a result, a variety of different solvent systems were investigated for self-assembly. Experiments were carried out as previously outlined for **1** and **2**.

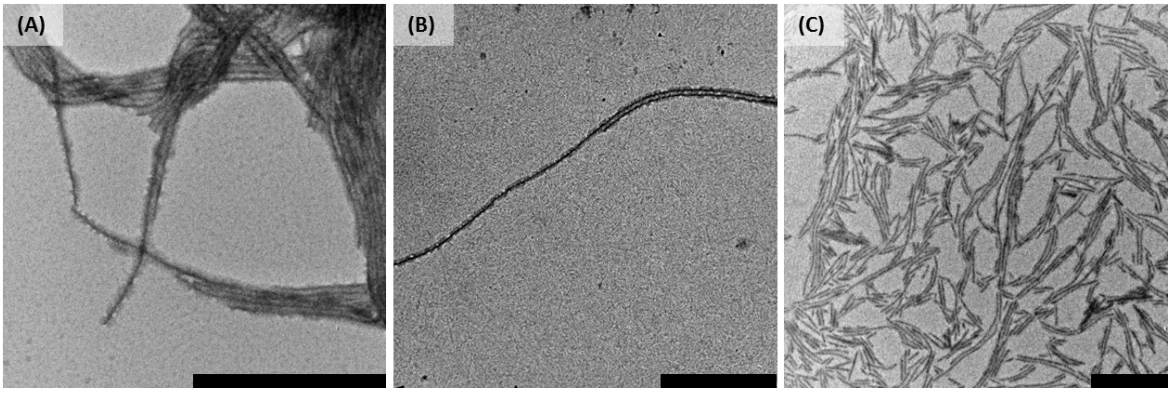


**Figure 11**: TEM micrographs of cylindrical triBCP micelles of **3** prepared in, and drop-cast from, (A) acetone, (B) acetone/EtOAc 1 : 1 (v/v) and (C) diglyme. TEM images after drying from solution taken at 0.1 mg/mL. Scale bars correspond to 1000 nm.

In pure EtOAc, BuOAc, hexanes or decane, films presumably derived from unimer of **3** were detected (Figure S30). In contrast, self-assembly in acetone afforded extensively aggregated cylindrical micelles after solvent evaporation (Figure 11A). In an attempt to reduce the amount of aggregation, a mixed solvent system of acetone/EtOAc 1 : 1 (v/v) was used to make the solvent more favourable for both corona forming blocks. This was successful, as cylindrical micelles that were relatively well-dispersed were observed (Figure 11B). Furthermore, dimethylacetamide (DMAA) and diglyme were also explored, as they were expected to be selective solvents for the PS block. In DMAA, a mixed morphology of spheres and cylinders were detected (Figure S30E), whereas

cylindrical micelles exclusively form when diglyme is employed as the solvent (Figure 11C). In addition to this, the coronal microstructure was probed to determine whether patchy structures had been formed in the dry state (Figure S31, S32).

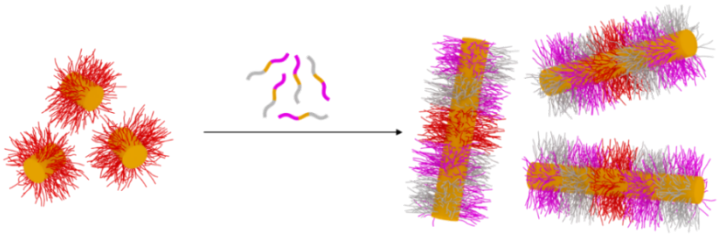

**Figure 12**: Schematic representation of the formation of block co-micelles of **3** grown off $PFDMS_{52}$-*b*-$PDMS_{414}$ seed micelles.

~~For the samples that afforded only cylindrical micelles, the coronal microstructure was probed to determine whether patchy structures had been formed. The samples did not need to be stained due to the presence of the long PS coronal chains which exhibited greater electron contrast by TEM compared to PMVS. The samples which contained acetone in the solvent system clearly showed the microphase separation between the PS and PMVS coronal chains, affording patchy materials (Figure S31A, S31B). The definition of the patches was much more prevalent when neat acetone was used compared to acetone/EtOAc 1 : 1 (v/v), which was a result of the solvent system being more selective for PS compared to PMVS. As the solvent quality increased for the PMVS block upon the addition of EtOAc, the definition of the patches decreased. Further acetone/EtOAc mixtures were investigated, showing that the definition of the patches was diminished as the EtOAc content increased (Figure S32). In contrast to this, samples prepared in diglyme showed no demarcation between the two corona forming blocks, affording structures with seemingly homogeneous mixing of PS and PMVS (Figure S31C).~~

Seeded growth experiments targeting controlled length cylindrical micelles of **3** were attempted in both acetone/EtOAc 1 : 1 (v/v) and diglyme (Figure 12). Seed micelles of both samples were prepared by sonicating 0.1 mg/mL samples at 0 °C for 2 h in an ultrasonic bath. Following this, known amounts of unimer of **3** were added to the seeds and the samples were left to age for 24 h.

Upon imaging of the samples in acetone/EtOAc 1 : 1 (v/v), the micelles had grown. However, the micelles aggregated considerably, which made analysis of the micelle contour lengths problematic to the point where statistical analysis was not possible (Figure S33). Moreover, despite the samples prepared in diglyme being well dispersed, the lengths of the micelles did not appear to increase upon the addition of further unimer (Figure S34). Polydisperse micelle samples were formed through either the spontaneous nucleation of **3**, or by the inactivity of a large fraction of the seed micelles to epitaxial growth.

In order to reduce the amount of micelle aggregation upon drying, the aforementioned $PFDMS_{52}$-*b*-$PDMS_{414}$ seed micelles ($L_n$ = 49 nm, $L_w/L_n$ = 1.10) in EtOAc were used instead of seeds prepared directly from **3**. Although direct micellisation of **3** in EtOAc did not take place (Figure S30A), seeded growth of **3** was possible ain this solvent as for the cases if **1** and **2**. Thus, when known amounts of unimer of **3** were added to $PFDMS_{52}$-*b*-$PDMS_{414}$ seed micelles and the samples were allowed to mature for a minimum of 72 h the resulting cylinders were shown to grow linearly as the unimer-to-seed ratio increased, and micelles up to ca. 1100 nm with low length dispersities ($L_w/L_n$ < 1.1) were prepared (Figure 13, S35). The lengths of the micelles correlated with the predicted micelle lengths depending on the amount of unimer added, indicative of a living CDSA process (Figure 13D~~F~~, Figure S36). In addition, the phase separation in the dry state between the PS and PMVS corona-forming blocks was still detected by TEM and AFM (Figure S35, Figure S37), yielding block co-micelles with a patchy structure.

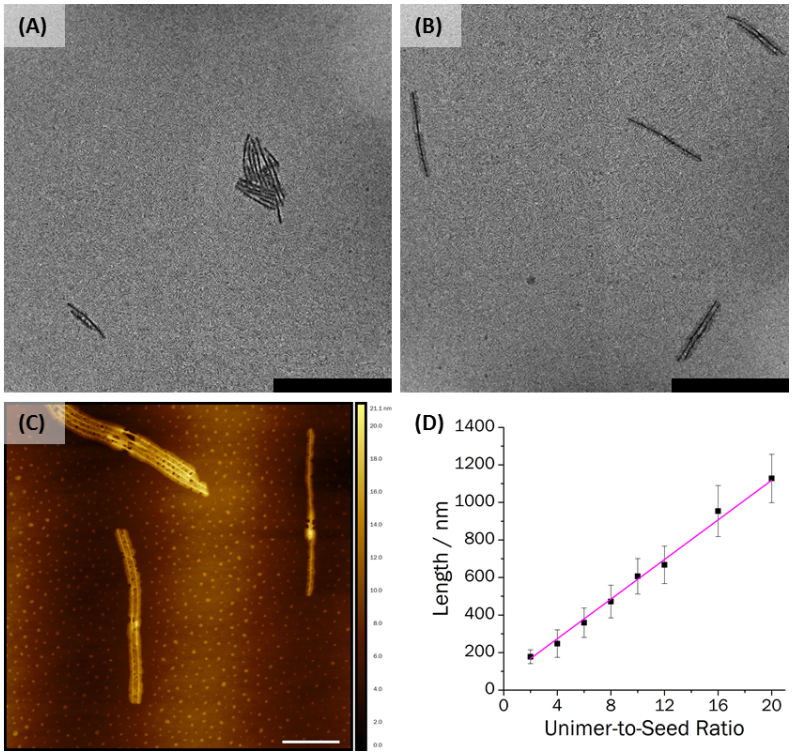


**Figure 13**: TEM micrographs of triBCP cylindrical block co-micelles prepared by seeded growth of **3** from $PFDMS_{52}$-*b*-$PDMS_{414}$ seed micelles ($L_n$ = 49 nm, $L_w/L_n$ = 1.10) in EtOAc after the addition of (A) 4 and (B) 12 equivalents of unimer; (C) AFM height micrograph of cylindrical block co-micelles after the addition of 20 equivalents of unimer; (D) Graph showing the linear dependence of micelle length upon the unimer-to-seed ratio. TEM and AFM images taken after drying from solution at 0.1 mg/mL. Scale bars correspond to (A)-(B) 1000 nm, (C) 500 nm.

**Summary**

Three different triBCPs possessing a central crystallizable PFDMS block and chemically distinct A and C corona-forming blocks have been prepared by a combination of living anionic polymerization, living radical polymerization and CuAAC click chemistry. The self-assembly of two PIP-*b*-PFDMS-*b*-PMMA triBCPs **1** and **2** differed in similar solvent systems, which was attributed different lengths of their respective corona-forming blocks. For **1**, with long PIP and PMMA coronal chains, spheres and/or cylinders were formed depending on the ease of crystallization of the PFDMS core. Seed micelles could be employed to allow the formation of cylindrical micelles with well-controlled lengths and narrow length dispersities via the living CDSA method. Moreover, phase-separated coronae with alternating patches of PIP and PMMA along the length of the micelles was observed by TEM. For **2**, ~~bicontinuous~~ micellar networks, in addition to cylinders and platelets were

formed depending on the polarity of the solvent used and the resulting degree of PFDMS crystallization. Self-assembly of a PS-*b*-PFDMS-*b*-PMVS, **3**, which had a similar core: corona composition to **1**, afforded cylindrical micelles that also exhibited coronal phase separation in various solvent systems. Moreover, the length of these patchy micelles was readily controlled using seeded growth methods.

The self-assembly behaviour of PFDMS-containing triBCPs differs significantly from than that observed with simpler diBCPs. The added presence of two rather than one corona-forming block flanking the central crystallizable PFDMS segment lowers the propensity of the PFDMS to crystallize. Furthermore, the presence of two chemically distinct corona-forming blocks with different solubilities provides access to assemblies with a "patchy" corona and can lead to the observation of interesting drying effects such as the formation of coiled micelles The ability to tailor the size and regularity of patches on micellar nanostructures, as well as the preparation of novel 2D architectures using blending strategies with homopolymers will be studied in the future. Furthermore, we are looking at how the difference in the seed micelle composition (whether it be composed from a triBCP or a BCP) affects the self-assembly behaviour of the incoming unimer during living CDSA in much greater detail. We are also currently exploring methods to visualise these patchy, network or aggregated structures in solution, as well as functionalization of patchy cylindrical micelle architectures with nanoparticles to prepare hybrid materials with a variety of potential applications.

**References**


1. R. C. Hayward and D. J. Pochan, *Macromolecules*, 2010, **43**, 3577-3584.
2. F. H. Schacher, P. A. Rupar and I. Manners, *Angew. Chem., Int. Ed.*, 2012, **51**, 7898-7921.
3. Y. Mai and A. Eisenberg, *Chem. Soc. Rev.*, 2012, **41**, 5969-5985.
4. U. Tritschler, S. Pearce, J. Gwyther, G. R. Whittell and I. Manners, *Macromolecules*, 2017, **50**, 3439-3463.
5. C. M. Bates and F. S. Bates, *Macromolecules*, 2017, **50**, 3-22.
6. D. J. Lunn, J. R. Finnegan and I. Manners, *Chem. Sci.*, 2015, **6**, 3663-3673.
7. A. O. Moughton, M. A. Hillmyer and T. P. Lodge, *Macromolecules*, 2012, **45**, 2-19.
8. J.-F. Lutz and A. Laschewsky, *Macromol. Chem. Phys.*, 2005, **206**, 813-817.
9. J. Dupont and G. Liu, *Soft Matter*, 2010, **6**, 3654-3661.
10. Z. Li, E. Kesselman, Y. Talmon, M. A. Hillmyer and T. P. Lodge, *Science*, 2004, **306**, 98-101.
11. T. Jiang, L. Wang, S. Lin, J. Lin and Y. Li, *Langmuir*, 2011, **27**, 6440-6448.
12. Z. Zhang, C. Zhou, H. Dong and D. Chen, *Angew. Chem., Int. Ed.*, 2016, **55**, 6182-6186.

13. T. I. Lobling, O. Borisov, J. S. Haataja, O. Ikkala, A. H. Groschel and A. H. Muller, *Nat. Commun.*, 2016, **7**, 12097.
14. J. Cai, K. P. Mineart, X. Li, R. J. Spontak, I. Manners and H. Qiu, *ACS Macro Lett.*, 2018, **7**, 1040-1045.
15. A. H. Gröschel, A. Walther, T. I. Löbling, F. H. Schacher, H. Schmalz and A. H. E. Müller, *Nature*, 2013, **503**, 247-251.
16. D. J. Lunn, O. E. C. Gould, G. R. Whittell, D. P. Armstrong, K. P. Mineart, M. A. Winnik, R. J. Spontak, P. G. Pringle and I. Manners, *Nature Communications*, 2016, **7**, 12371.
17. T. L. Nghiem, T. I. Löbling and A. H. Gröschel, *Polymer Chemistry*, 2018, **9**, 1583-1592.
18. R. K. O'Reilly, C. J. Hawker and K. L. Wooley, *Chem. Soc. Rev.*, 2006, **35**, 1068-1083.
19. Z. Ge and S. Liu, *Chem. Soc. Rev.*, 2013, **42**, 7289-7325.
20. C. V. Synatschke, T. Nomoto, H. Cabral, M. Förtsch, K. Toh, Y. Matsumoto, K. Miyazaki, A. Hanisch, F. H. Schacher, A. Kishimura, N. Nishiyama, A. H. E. Müller and K. Kataoka, *ACS Nano*, 2014, **8**, 1161-1172.
21. R. Bahrami, T. I. Löbling, H. Schmalz, A. H. E. Müller and V. Altstädt, *Polymer*, 2015, **80**, 52-63.
22. R. Bahrami, T. I. Löbling, A. H. Gröschel, H. Schmalz, A. H. E. Müller and V. Altstädt, *ACS Nano*, 2014, **8**, 10048-10056.
23. T. Gegenhuber, M. Krekhova, J. Schöbel, A. H. Gröschel and H. Schmalz, *ACS Macro Lett.*, 2016, **5**, 306-310.
24. A. H. Groschel and A. H. Muller, *Nanoscale*, 2015, **7**, 11841-11876.
25. J. Schobel, M. Burgard, C. Hils, R. Dersch, M. Dulle, K. Volk, M. Karg, A. Greiner and H. Schmalz, *Angew. Chem., Int. Ed.*, 2017, **56**, 405-408.
26. J. Wang, W. Li and J. Zhu, *Polymer*, 2014, **55**, 1079-1096.
27. J. A. Massey, K. Temple, L. Cao, Y. Rharbi, J. Raez, M. A. Winnik and I. Manners, *J. Am. Chem. Soc.*, 2000, **122**, 11577-11584.
28. L. Cao, I. Manners and M. A. Winnik, *Macromolecules*, 2002, **35**, 8258-8260.
29. J. Schmelz, M. Karg, T. Hellweg and H. Schmalz, *ACS Nano*, 2011, **5**, 9523-9534.
30. J. Xu, H. Zhou, Q. Yu, I. Manners and M. A. Winnik, *J. Am. Chem. Soc.*, 2018, **140**, 2619-2628.
31. W.-N. He and J.-T. Xu, *Prog. Polym. Sci.*, 2012, **37**, 1350-1400.
32. W.-N. He, B. Zhou, J.-T. Xu, B.-Y. Du and Z.-Q. Fan, *Macromolecules*, 2012, **45**, 9768-9778.
33. A. Pitto-Barry, N. Kirby, A. P. Dove and R. K. O'Reilly, *Polym. Chem.*, 2014, **5**, 1427-1436.
34. C. Legros, M. C. De Pauw-Gillet, K. C. Tam, D. Taton and S. Lecommandoux, *Soft Matter*, 2015, **11**, 3354-3359.
35. J. Schmelz, F. H. Schacher and H. Schmalz, *Soft Matter*, 2013, **9**, 2101-2107.
36. S.-J. Park, S.-G. Kang, M. Fryd, J. G. Saven and S.-J. Park, *J. Am. Chem. Soc.*, 2010, **132**, 9931-9933.
37. J. Qian, X. Li, D. J. Lunn, J. Gwyther, Z. M. Hudson, E. Kynaston, P. A. Rupar, M. A. Winnik and I. Manners, *J. Am. Chem. Soc.*, 2014, **136**, 4121-4124.
38. E. L. Kynaston, O. E. C. Gould, J. Gwyther, G. R. Whittell, M. A. Winnik and I. Manners, *Macromol. Chem. Phys.*, 2015, **216**, 685-695.
39. M. E. Robinson, D. J. Lunn, A. Nazemi, G. R. Whittell, L. De Cola and I. Manners, *Chem. Commun.*, 2015, **51**, 15921-15924.
40. S. Ogi, K. Sugiyasu, S. Manna, S. Samitsu and M. Takeuchi, *Nat. Chem.*, 2014, **6**, 188-195.
41. X. Wang, G. Guerin, H. Wang, Y. Wang, I. Manners and M. A. Winnik, *Science*, 2007, **317**, 644-647.
42. J. B. Gilroy, T. Gädt, G. R. Whittell, L. Chabanne, J. M. Mitchels, R. M. Richardson, M. A. Winnik and I. Manners, *Nat. Chem.*, 2010, **2**, 566-570.
43. Z. M. Hudson, C. E. Boott, M. E. Robinson, P. A. Rupar, M. A. Winnik and I. Manners, *Nat. Chem.*, 2014, **6**, 893-898.
44. A. M. Oliver, J. Gwyther, M. A. Winnik and I. Manners, *Macromolecules*, 2018, **51**, 222-231.
45. J. R. Finnegan, D. J. Lunn, O. E. Gould, Z. M. Hudson, G. R. Whittell, M. A. Winnik and I. Manners, *J. Am. Chem. Soc.*, 2014, **136**, 13835-13844.

46. A. Nunns, G. R. Whittell, M. A. Winnik and I. Manners, *Macromolecules*, 2014, **47**, 8420-8428.
47. H. Qiu, Y. Gao, C. E. Boott, O. E. C. Gould, R. L. Harniman, M. J. Miles, S. E. D. Webb, M. A. Winnik and I. Manners, *Science*, 2016, **352**, 697-701.
48. H. Qiu, Z. M. Hudson, M. A. Winnik and I. Manners, *Science*, 2015, **347**, 1329-1332.
49. X. Li, Y. Gao, C. E. Boott, M. A. Winnik and I. Manners, *Nat. Commun.*, 2015, **6**, 8127.
50. R. L. N. Hailes, A. M. Oliver, J. Gwyther, G. R. Whittell and I. Manners, *Chemical Society Reviews*, 2016, **45**, 5358-5407.
51. J. Schmelz, A. E. Schedl, C. Steinlein, I. Manners and H. Schmalz, *J. Am. Chem. Soc.*, 2012, **134**, 14217-14225.
52. N. Petzetakis, A. P. Dove and R. K. O'Reilly, *Chem. Sci.*, 2011, **2**, 955-960.
53. M. C. Arno, M. Inam, Z. Coe, G. Cambridge, L. J. Macdougall, R. Keogh, A. P. Dove and R. K. O'Reilly, *J. Am. Chem. Soc.*, 2017, **139**, 16980-16985.
54. X. Li, P. J. Wolanin, L. R. MacFarlane, R. L. Harniman, J. Qian, O. E. C. Gould, T. G. Dane, J. Rudin, M. J. Cryan, T. Schmaltz, H. Frauenrath, M. A. Winnik, C. F. J. Faul and I. Manners, *Nat. Commun.*, 2017, **8**, 15909.
55. E. L. Kynaston, A. Nazemi, L. R. MacFarlane, G. R. Whittell, C. F. J. Faul and I. Manners, *Macromolecules*, 2018, **51**, 1002-1010.
56. S. Shin, F. Menk, Y. Kim, J. Lim, K. Char, R. Zentel and T.-L. Choi, *Journal of the American Chemical Society*, 2018, **140**, 6088-6094.
57. L. Han, M. Wang, X. Jia, W. Chen, H. Qian and F. He, *Nature Communications*, 2018, **9**, 865.
58. D. Tao, C. Feng, Y. Cui, X. Yang, I. Manners, M. A. Winnik and X. Huang, *Macromolecules*, 2018, **51**, 2065-2075.
59. X.-H. Jin, M. B. Price, J. R. Finnegan, C. E. Boott, J. M. Richter, A. Rao, S. M. Menke, R. H. Friend, G. R. Whittell and I. Manners, *Science*, 2018, **360**, 897-900.
60. W. Zhang, W. Jin, T. Fukushima, A. Saeki, S. Seki and T. Aida, *Science*, 2011, **334**, 340-343.
61. A. Aliprandi, M. Mauro and L. De Cola, *Nat. Chem.*, 2016, **8**, 10-15.
62. Y. Liu, C. Peng, W. Xiong, Y. Zhang, Y. Gong, Y. Che and J. Zhao, *Angew. Chem., Int. Ed.*, 2017, **56**, 11380-11384.
63. H. Schmalz, J. Schmelz, M. Drechsler, J. Yuan, A. Walther, K. Schweimer and A. M. Mihut, *Macromolecules*, 2008, **41**, 3235-3242.
64. J. Schöbel, M. Karg, D. Rosenbach, G. Krauss, A. Greiner and H. Schmalz, *Macromolecules*, 2016, **49**, 2761-2771.
65. H. Wang, W. Lin, K. P. Fritz, G. D. Scholes, M. A. Winnik and I. Manners, *J. Am. Chem. Soc.*, 2007, **129**, 12924-12925.
66. H. Wang, A. J. Patil, K. Liu, S. Petrov, S. Mann, M. A. Winnik and I. Manners, 2009, **21**, 1805-1808.
67. F. Qi, G. Guerin, G. Cambridge, W. Xu, I. Manners and M. A. Winnik, *Macromolecules*, 2011, **44**, 6136-6144.
68. C. E. Boott, E. M. Leitao, D. W. Hayward, R. F. Laine, P. Mahou, G. Guerin, M. A. Winnik, R. M. Richardson, C. F. Kaminski, G. R. Whittell and I. Manners, *ACS Nano*, 2018, **12**, 8920-8933.
69. V. Abetz, R. J. Spontak and Y. Talmon, in *Macromolecular Engineering: Precise Synthesis, Materials Properties, Applications*, Wiley-VCH, Weinheim, 2007, vol. 3, ch. 7, pp. 1649-1685.
70. H. Jinnai and R. J. Spontak, *Polymer*, 2009, **50**, 1067-1087.
71. H. Jinnai, R. J. Spontak and T. Nishi, *Macromolecules*, 2010, **43**, 1675-1688.
72. R. A. Crowther, D. J. DeRosier and A. Klug, 1970, **317**, 319-340.
73. L. Shen, H. Wang, G. Guerin, C. Wu, I. Manners and M. A. Winnik, *Macromolecules*, 2008, **41**, 4380-4389.

**Table of Contents**